Compatibility of Steels in Supercritical CO_2 at 450°-650°C

B. A. Pint, R. Pillai and J. R. Keiser
Corrosion Science and Technology Group, Materials Science and Technology Division
Oak Ridge National Laboratory, Oak Ridge, TN 37831-6156 USA

ABSTRACT

Supercritical CO_2 (sCO_2) power cycles, particularly direct-fired cycles, have the possibility of revolutionizing clean fossil energy. However, in the lower temperature sections of the cycle, lower cost steels are needed in order to lower the cost of the sCO_2 technology. Representative 9 and 12%Cr steels and conventional and advanced austenitic steels are being evaluated at 450-650°C using mass change, bulk carbon (C) content and room temperature tensile properties to determine the maximum use temperatures for both direct- and indirect-fired sCO_2 cycles. After 1000 h exposures in research grade (RG) sCO_2 at 300 bar and RG sCO_2 with 1% O_2 and 0.1% H_2O additions, the results suggest that increasing the Cr content from 9 to 12% yielded no signficant benefit under these conditions but the higher Cr and Ni contents in S31025 provided better compatibility in RG sCO_2 at 650°C but limited benefit at 550°C with impurities. For S31609, the formation of Fe-rich oxide after exposure to RG sCO_2 at 650°C resulted in both an increase in the bulk C content and a large drop in room temperature ductility. The evidence suggests thin, protective oxides prevented C ingress in these conditions.

Keywords: supercritical carbon dioxide, thermal cycling, lifetime model

INTRODUCTION

Several power generation technologies are exploring the use of supercritical CO_2 (sCO_2) including fossil, nuclear, geothermal, concentrating solar power (CSP) and waste heat recovery, because of its unique properties and relatively low critical point (31°C/73.8 bar)[1-6]. Several recent studies focused on sCO_2 operating temperatures of ≥700°C[7-12], where greater than 50% thermal efficiency is predicted[13]. However, for sCO_2-based cycles to be commercially competitive, lower cost steels are needed in the lower temperature components in the cycle. There is concern about the use of steels in sCO_2 because prior experience of K90941 (Grade 9) in the UK advanced gas cooled reactors (AGRs) operated with 43 bar CO_2 (sub-critical conditions) at ≤550°C where severe internal carburization could occur under those conditions[14]. A recent review concluded that creep-strength enhanced ferritic (CSEF) steels were

limited to 450°C in sCO_2[15], significantly lower than the 580°-600°C limit in supercritical steam[16]. A nuclear fuel cladding study found that a stainless steel such as S32750 (type 316FR) had much better oxidation resistance than 9-12%Cr CSEF steels but began to show accelerated oxidation at 600°C[17]. Another factor in assessing sCO_2 steel compatibility is the presence of impurities in the sCO_2. At 750°C, little difference in reaction rates was noted between research grade (RG) sCO_2 and industrial grade sCO_2[10]. However, the higher impurity levels expected for direct-fired cycles[3,5], compared to indirect-fired or closed cycles, has been shown to affect reaction rates[8,10]. Also, the additions (CH_4, H_2O, etc.) in the AGR CO_2 used to prevent oxidation of the graphite moderator may have affected performance.

The current work has exposed two CSEF steels and two austenitic steels to 300 bar RG sCO_2 at 450°-650°C for 1000 h (two 500-h cycles) to begin to determine the maximum use temperatures for these materials. An initial 1000 h experiment also has been conducted at 550°C with controlled O_2 and H_2O additions[10] to simulate the Allam cycle. In addition to mass change and oxide thickness, room temperature tensile properties and bulk C content[18,19] have been measured to assess internal carburization.

EXPERIMENTAL PROCEDURE

The chemical composition of the four steels investigated in this study are shown in Table 1. Alloy coupons (~12 x 20 x 1.5mm) were polished to a 600 grit finish and tensile specimens (SS-3 type: 25.4 mm long, 0.76 x 5 mm gauge) were prepared with a similar finish. All specimens were ultrasonically cleaned in acetone and methanol prior to exposure. For the 500-h cycles in 300 bar RG sCO_2, the exposures were conducted in an autoclave fabricated from N07208. The vertically-oriented autoclave (~266 mm x 83 mm inner diameter) was operated inside a three-zone furnace with an N07208 sample rack that sat on the bottom of the autoclave. The fluid flow rate was ~2 ml/min and additional details are provided elsewhere[9,10,20]. The specimens were slowly heated to temperature over several hours (~2°C/min) in sCO_2, held at temperature ±2°C and then cooled in sCO_2 to room temperature using a cooling fan on the autoclave. For the controlled impurity sCO_2 experiments, three pumps were used for the sCO_2, O_2, and H_2O, and the O_2 was delivered as a CO_2–O_2 gaseous mixture. The O_2 was calculated (based on gas flow) as 1.0 ± 0.2% and the H_2O content as 0.1 ± 0.05% with most of the variation associated with the change in sCO_2 cylinders (typically twice per 500-h cycle) and operational issues such as filter plugging and valve leakage.

Before and after each 500-h cycle, the specimens were weighed using a Mettler Toledo XP205 balance with an accuracy of ±0.04 mg or ~0.01 mg/cm^2. After exposure, tensile specimens were tested at room

Table 1
Alloy chemical compositions (weight %)(1)

Alloy	UNS#	Fe	Cr	Ni	Mo	Mn	Si	C	S(ppm)	Other
Gr.91	K90901	88.8	8.6	0.3	0.9	0.46	0.35	0.10	6	0.2V,0.06Nb,0.045N
12CrCoW		83.3	11.5	0.4	0.4	0.38	0.42	0.12	3	1.6W,1.5Co,0.2V,0.04N
316H	S31609	69.5	16.3	10.0	2.0	0.84	0.46	0.041	6	0.3Cu,0.3Co,0.04N
709	S31025	51.3	20.1	25.2	1.5	0.89	0.41	0.064	3	0.2Nb,0.06Cu,0.15N

(1) measured by inductively coupled plasma analysis and combustion analysis
< indicates below the detectability limit of <0.01%

temperature with a strain rate of 0.015/min per ASTM E8-13. The bulk C uptake was measured using combustion analysis. For metallography, specimens were Cu plated before sectioning. Reaction product thickness was measured using image analysis software with ~30 measurements per specimen.

RESULTS

Figure 1 shows the coupon mass change data in 300 bar RG sCO_2. Box and whiskers are used to show the results from 5-6 specimens of each alloy at each condition and the median values are shown. One specimen of each alloy was removed after each cycle for characterization. As expected, the 9-12%Cr steels showed higher mass gains at each temperature. At 650°C, scale spallation was evident for these specimens which affected the values and distribution, Figure 1b. The two median data points were used to calculate parabolic rate constants by plotting them vs. the square root of time[21]. Figure 2 shows that the rates (large open symbols) were very similar to those previously measured[17] and changing from 8.6% to 11.5% Cr had little effect on the rates in this temperature range where Cr mobility is limited[22]. For the stainless steels, the mass gain were very low at 450° and 550°C and only the 550°C mass gains are shown in Figure 1a. At 650°C, the mass gains also were very low for the S31025 specimens. However, a much thicker oxide was observed for the S31609 specimens, which also is consistent with prior work[17,23]. The rates for S31609 were consistent with prior literature values[17], Figure 2. No prior results were found for S31025 in sCO_2 but the rates near 10^{-16} g^2/cm^4s are as low as can be measured with 0.01 mg/cm^2 accuracy and are similar to rates measured for chromia-forming Ni-based alloys[24].

Figure 3 shows the mass change data at 550°C with and without controlled impurity additions. The shaded boxes show the results with 1%O_2+0.1%H_2O additions. For the CSEF steels, no statistically significant change in mass gain was observed with the addition of impurities. In contrast, both austenitic steels experienced higher mass gains. The larger change for the S31025 specimens was observed after the second 500-h cycle. After the first cycle, median values of 0.02 mg/cm^2 were measured in both conditions. The measured rates are shown as closed symbols at 550°C in Figure 2.

To avoid relying solely on mass change data, specimens were removed from these experiments after each cycle for characterization of the reaction products. Figure 4 shows examples of the reaction products for each alloy after one 500-h cycle at each condition. Consistent with the mass change data

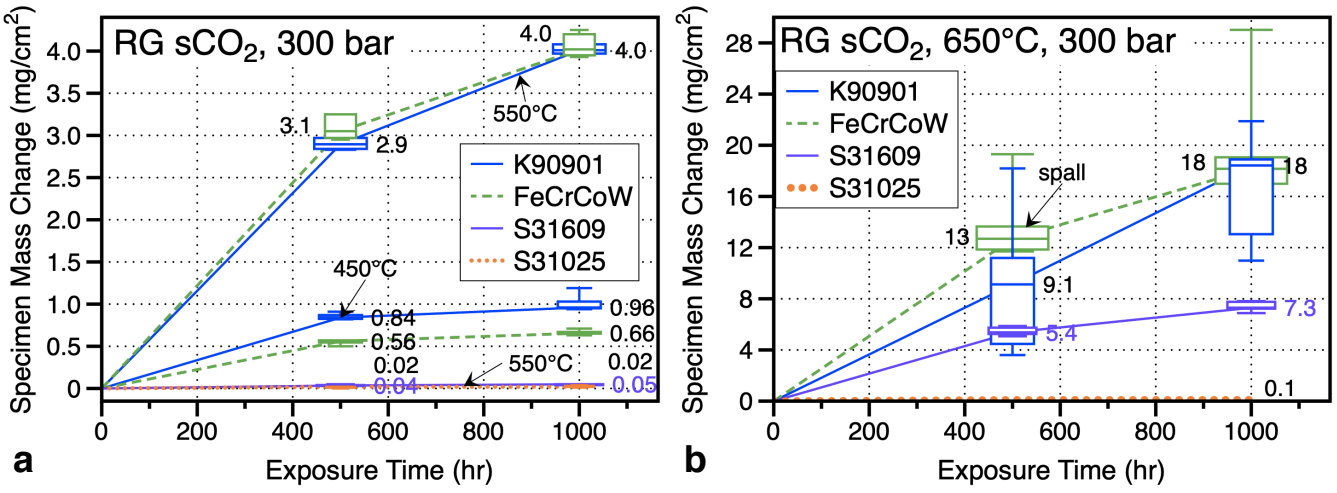

Figure 1. Specimen mass gain during 500-h cycles in 300 bar RG sCO_2 (a) 450° and 550°C and (b) 650°C. Box and whisker plots show data for 5-6 specimens exposed and the median values are shown.

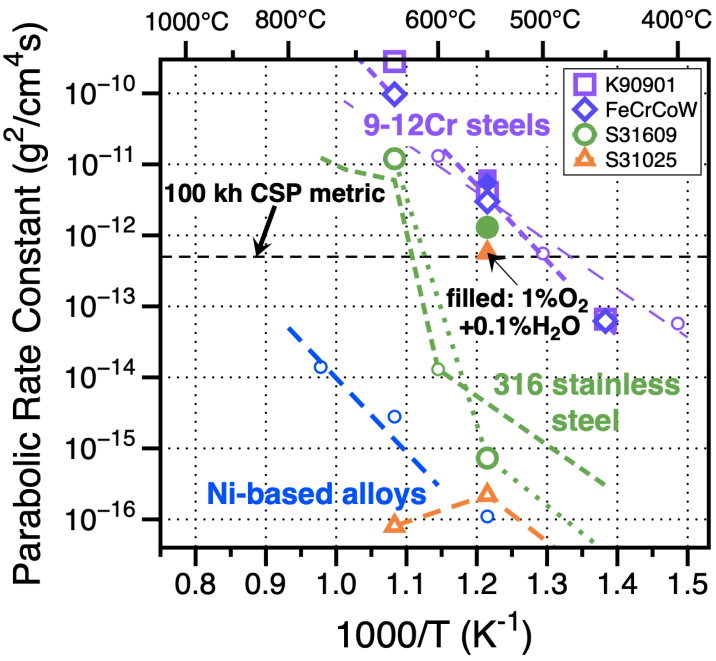

Figure 2: Arrhenius plot of literature values and rate constants from this study in 300 bar RG CO_2 (open symbols) and RG sCO_2 with 1%O_2 + 0.1%H_2O (solid symbols).

at 450°C, a much thicker scale was observed on the K90901 and FeCrCoW specimens than on the higher alloyed austenitic steels. Figure 5 shows oxide scale measurements for the scales formed at each condition. The scales were thicker after a similar exposure at 550°C in RG sCO_2, Figure 4b. At this magnification it is easier to see the duplex Fe-rich oxide microstructure formed on the 9-12%Cr steels as well as an internal oxidation layer at the metal-oxide interface. The light microscopy images show a contrast between the outer magnetite layer and the inner $(Fe,Cr)_3O_4$ layer that has been previously identified[16,25,26]. A thin protective Cr-rich oxide was observed on the austenitic steels at 550°C in RG sCO_2.

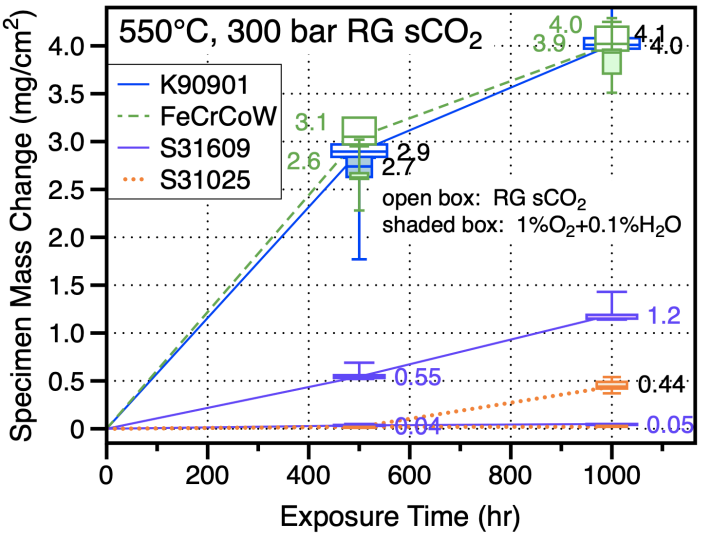

Figure 3. Specimen mass gain during 500-h cycles at 550°C in 300 bar RG sCO_2 and RG sCO_2 with 1%O_2 and 0.1%H_2O.

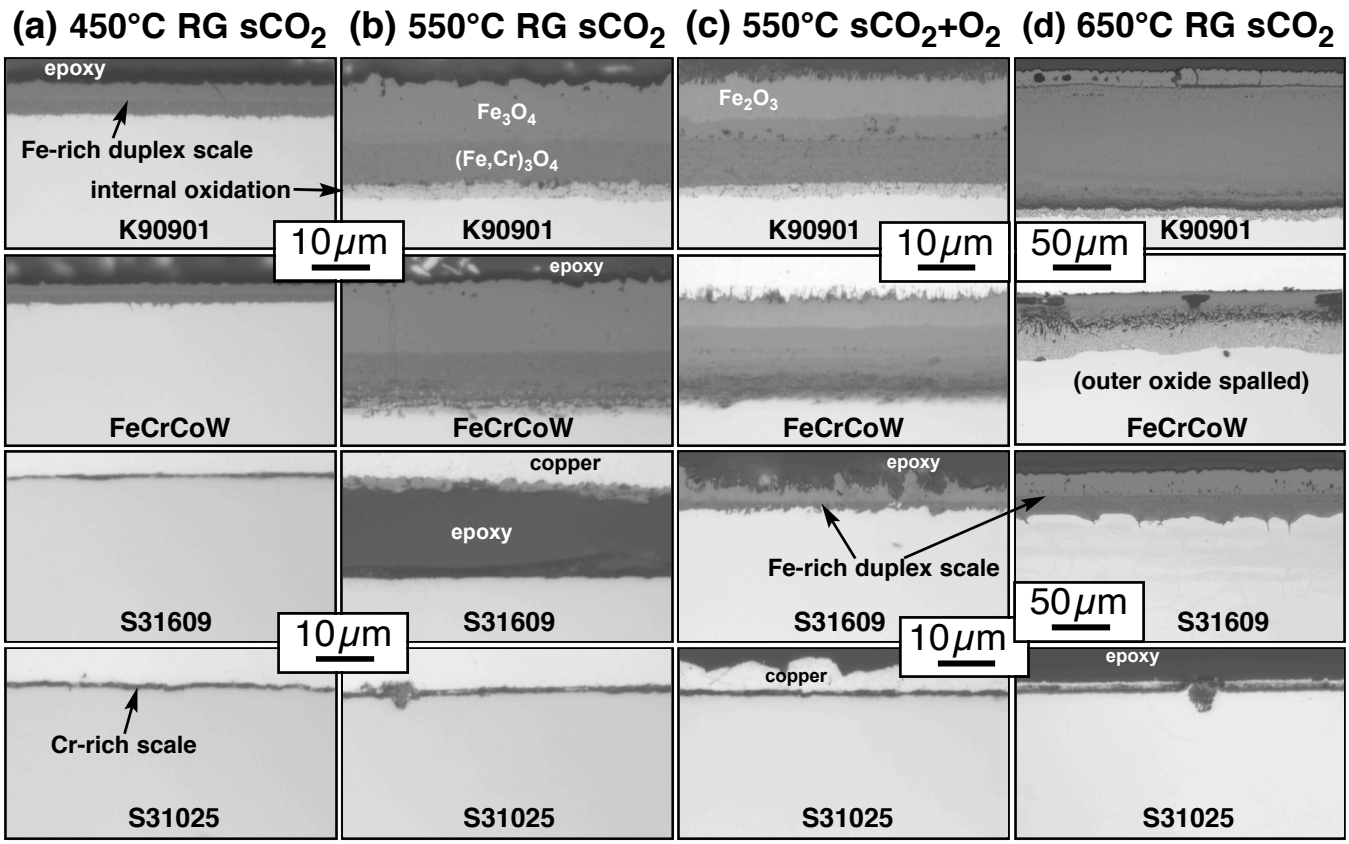

Figure 4: Light microscopy of polished cross-sections of specimens of four steels after 500 h exposures in 300 bar RG sCO_2 (a) 450°C, (b) 550°C, (c) 550°C with 1%O_2+0.1%H_2O and (d) 650°C.

With the addition of impurities at 550°C, the reaction products were similar for three of the alloys, Figures 4b and 4c. After 500 h, a thin protective oxide was observed with and without impurities for the S31025 specimens. While the reaction products were similar in thickness for the K90901 and FeCrCoW specimens, the lighter scale layer indicated the formation of an outermost hematite layer. The most distinctive difference occurred for the S31609 specimens, where a thicker duplex scale formed with the addition of impurities. As noted previously, at 650°C, scale spallation was an issue for the CSEF steels,

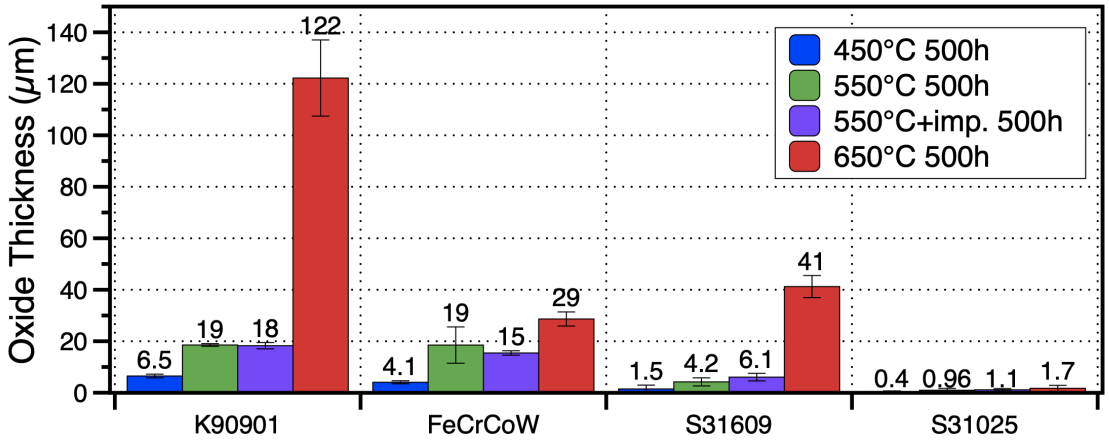

Figure 5: Average oxide thickness after 500 h exposure in 300 bar RG CO_2 at each condition. The whiskers show one standard deviation.

Figure 4d. A lower magnification was needed for the steels forming Fe-rich oxides at this temperature including the S31609 specimen. A thin protective oxide continued to form on the S31025 specimen under these conditions, however, occasional disruptions were observed. Additional characterization of these specimens is in progress.

Figure 6a compares the room temperature tensile properties of the alloys after 500 h exposures at each temperature with the as-received properties. In many cases, the results were very similar before and after exposure. The most striking change was for the S31609 specimen exposed at 650°C where a large drop in total elongation was observed along with an increase in the yield strength. Both changes are indicative of internal carburization[18]. Figure 6b compares the as-received properties to 1000 h exposures to RG sCO_2 with and without impurities. In addition, measurements for specimens that were annealed for 1000 h in an inert atmosphere are shown. For both austenitic steels, a drop in yield strength was observed after exposure to the high impurity environment. A drop in yield strength also was observed for thermally annealed S31609 specimen.

Finally, Figure 7 shows the bulk C contents measured for specimens exposed 1000 h at each condition. The C contents in Table 1 were measured using the same procedure. The largest increases were observed at 650°C for the three alloys that formed Fe-rich oxides. No increase was observed for S31025 specimens in any condition supporting the hypothesis that chromia scales can prevent C ingress[27] and contradicting results for model Fe-Cr alloys[28]. In the high impurity environment, a larger increase in C was observed for the K90901 specimen from 0.10 wt.% to 0.13% C, compared to 0.11% without impurities.

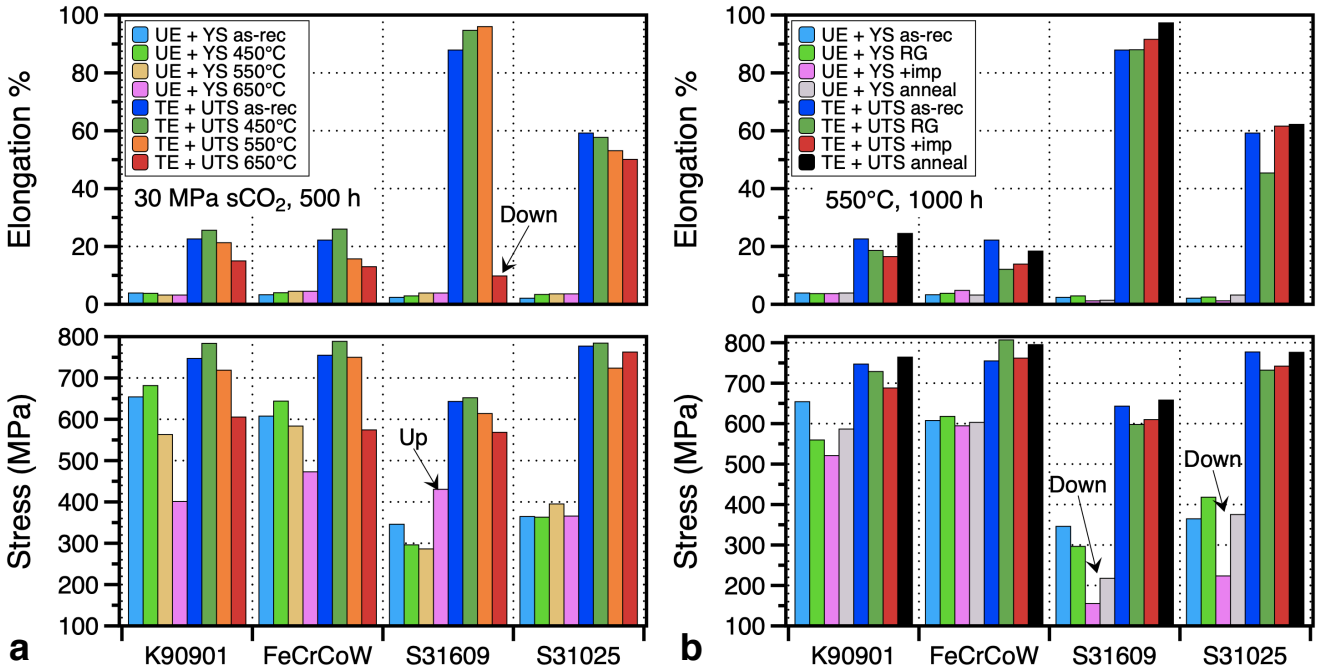

Figure 6: Room temperature tensile properties of steels (a) before and after 500 h exposures in RG sCO_2 and (b) before and after 1000 h exposures at 550°C in RG sCO_2 with and without impurities compared to a thermal anneal.

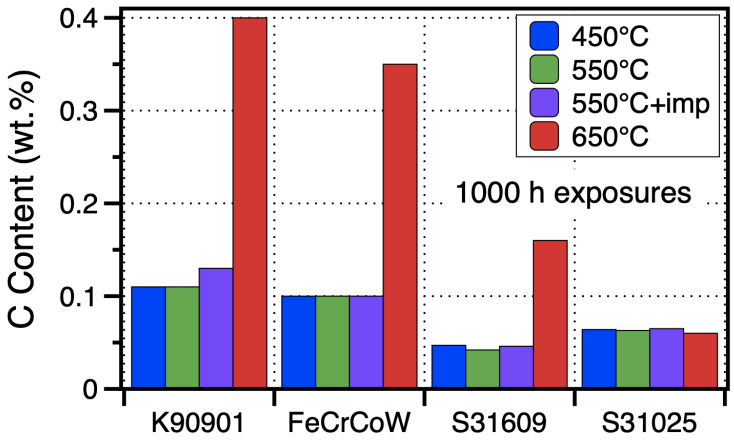

Figure 7: Alloy C content measured after 1000 h exposures in each environment using combustion analysis.

DISCUSSION

By combining several methodologies, a consistent picture is being created that when a thin protective scale forms, the steels retain good mechanical properties and no C ingress is detected. The results indicate that increasing the Cr content from 9 to 12% did not yield any significant benefit in performance. The higher Cr and Ni content in S31025 did appear to be beneficial at 650°C in terms of a much slower reaction rate (Figure 2) and no C ingress (Figure 7). However, the benefit did not appear to extend to impure sCO_2 at 550°C, where a large mass gain was measured after 500 h, suggesting a rapid rate.

While the results are clear at 650°C, longer exposures at 550°C may be very useful in observing the evolution in reaction products and tensile properties. Unfortunately, the remaining 550°C specimens were damaged by a power outage during a third cycle in RG sCO_2 and a new set of specimens will need to be restarted to investigate longer times at 550°C. While two data points may not provide an accurate rate constant calculation in all cases, in the previous 10,000 h study at 750°C, the rates determined after 2 cycles were very similar to those calculated after 20 cycles[12]. However, for S31025, the mass gains were so low that longer times may be needed to calculate more accurate rates in RG sCO_2 and in impure sCO_2, the mass gain increase between 500 and 1000 h may reflect only transient behavior with longer exposures needed to define steady-state rates.

The parabolic rate constant metric shown in Figure 2 was used as an estimate for when scale spallation might be expected to be significant for a 100,000 h CSP lifetime[12]. The metric was developed for Ni-based Cr-forming scales but may be somewhat relevant for these alloys. The low rates observed for S31025 in RG sCO_2 are unlikely to lead to scale spallation at long exposure times. However, the thicker Fe-rich scales formed on the CSEF steels, even at 450°C, may eventually spall at long times.

The duplex Fe-rich oxides have been observed many times and in many different environments including those containing CO_2 and H_2O[9,14-18,23,25,26,28-31]. The outer layer remaining magnetite in RG sCO_2 is consistent with the low pO_2 in the sCO_2 environment[9]. With the addition of 1%O_2, the pO_2 increased to 0.01 and hematite formed, Figure 4c.

Currently, the specimen characterization remains incomplete and several assumptions about scale composition need to be confirmed. In addition etching (e.g. with aqua regia) is needed at 450° and 550°C to determine if an internal carburization zone has formed in these materials. Future work will

continue to expose these materials in impure sCO_2 at 450° and 650°C to determine a more complete understanding about the role of impurities on sCO_2 compatibility.

SUMMARY

The sCO_2 compatibility of four steels was investigated in (RG) sCO_2 at 300 bar at 450°-650°C and RG sCO_2 with 1% O_2 and 0.1% H_2O additions at 550°C. Mass change was used to calculate parabolic reaction rates and post-exposure bulk C content and room temperature tensile properties also were measured. After these 1000 h exposures, there was no apparent benefit of increasing the Cr content from 9 to 12% in ferritic-martensitic steels. However, the higher Cr and Ni contents in S31025 provided better compatibility in RG sCO_2 at 650°C but limited benefit at 550°C with impurities. For S31609, the formation of Fe-rich oxide after exposure to RG sCO_2 at 650°C resulted in both an increase in the bulk C content and a large drop in room temperature ductility. The evidence suggests thin, protective oxides prevented C ingress in these conditions and thick Fe-rich oxides allowed C ingress.

ACKNOWLEDGMENTS

The authors would like to thank B. Johnston, M. Howell, T. M. Lowe and V. Cox for assistance with the experimental work at ORNL. E. Lara-Curzio and M. J. Lance provided helpful comments on the manuscript. This research was sponsored by the U.S. Department of Energy, Office of Fossil Energy, Crosscutting Technology Program. This manuscript has been authored by UT-Battelle, LLC under Contract No. DE-AC05-00OR22725 with the U.S. Department of Energy. The United States Government retains and the publisher, by accepting the article for publication, acknowledges that the United States Government retains a non-exclusive, paid-up, irrevocable, world-wide license to publish or reproduce the published form of this manuscript, or allow others to do so, for United States Government purposes. The Department of Energy will provide public access to these results of federally sponsored research in accordance with the DOE Public Access Plan (http://energy.gov/downloads/doe-public-access-plan).

REFERENCES

1. V. Dostal, P. Hejzlar and M. J. Driscoll, “The supercritical carbon dioxide power cycle: Comparison to other advanced power cycles,” Nucl. Technol. 154, 3 (2006): pp.283-301.
2. H. Chen, D. Y. Goswami and E. K. Stefanakos, “A review of thermodynamic cycles and working fluids for the conversion of low-grade heat,” Renewable & Sustainable Energy Reviews 14 (2010): pp.3059-3067.
3. R. J. Allam, M. R. Palmer, G. W. Brown Jr., J. Fetvedt, D. Freed, H. Nomoto, M. Itoh, N. Okita, C. Jones Jr., “High efficiency and low cost of electricity generation from fossil fuels while eliminating atmospheric emissions, including carbon dioxide,” Energy Procedia 37 (2013): pp.1135–1149.
4. B. D. Iverson, T. M. Conboy, J. J. Pasch and A. M. Kruizenga, “Supercritical CO_2 Brayton cycles for solar-thermal energy,” Applied Energy 111, (2013): pp.957-970.
5. I. G. Wright, B. A. Pint, J. P. Shingledecker and D. Thimsen, (2013) “Materials Considerations for Supercritical CO_2 Turbine Cycles,” ASME Paper #GT2013-94941, presented at the International Gas Turbine & Aeroengine Congress & Exhibition, San Antonio, TX, June 3-7, 2013.
6. V. T. Cheang, R. A. Hedderwick, C. McGregor, “Benchmarking supercritical CO_2 cycles against steam Rankine cycles for Concentrated Solar Power,” Solar Energy 113 (2015): pp.199-211.

7. R. I. Olivares, D. J. Young, P. Marvig and W. Stein, “Alloys SS316 and Hastelloy-C276 in Supercritical CO_2 at High Temperature,” Oxid. Met. 84 (2015): pp.585–606.
8. J. Mahaffey, D. Adam, A. Brittan, M. Anderson and K. Sridharan, “Corrosion of Alloy Haynes 230 in High Temperature Supercritical Carbon Dioxide with Oxygen Impurity Additions,” Oxidation of Metals 86 (2016): pp.567-580.
9. B. A. Pint, R. G. Brese and J. R. Keiser, “Effect of Pressure on Supercritical CO_2 Compatibility of Structural Alloys at 750°C,” Materials and Corrosion 68 (2017): pp.151-158.
10. B. A. Pint, J. Lehmusto, M. J. Lance and J. R. Keiser, “The Effect of Pressure and Impurities on Oxidation in Supercritical CO_2,” Mater. Corros. 70 (2019): pp.1400-1409.
11. R. P. Oleksak, J. H. Tylczak, C. S. Carney, G. R. Holcomb and O. N. Dogan, “High-Temperature Oxidation of Commercial Alloys in Supercritical CO_2 and Related Power Cycle Environments,” JOM 70 (2018): pp.1527-1534.
12. B. A. Pint, R. Pillai, M. J. Lance and J. R. Keiser “Effect of Pressure and Thermal Cycling on Long-Term Oxidation in CO_2 and Supercritical CO_2” Oxidation of Metals 94 (2020): pp.505–526.
13. E. G. Feher, “The Supercritical Thermodynamic Power Cycle,” Energy Conversion, 8 (1968): pp.85-90.
14. Y. Gong, D. J. Young, P. Kontis, Y. L. Chiu, H. Larsson, A. Shin, J. M. Pearson, M. P. Moody and R. C. Reed, “On the breakaway oxidation of Fe9Cr1Mo steel in high pressure CO_2,” Acta Materialia, 130 (2017): pp.361-374.
15. S. Sarrade, D Férona, F. Rouillard, S. Perrin, R. Robin, J.-C. Ruiz, H.-A. Turc, “Overview on corrosion in supercritical fluids,” Journal of Supercritical Fluids, 120 (2017): pp.335–344.
16. J. P. Shingledecker, B.A. Pint, A.S. Sabau, A.T. Fry and I.G. Wright, “Managing Steam-Side Oxidation and Exfoliation in USC Boiler Tubes,” Advanced Materials and Processing, 171(1) (2013): pp.23-25.
17. T. Furukawa, Y. Inagaki, M. Aritomi, “Compatibility of FBR structural materials with supercritical carbon dioxide,” Progress in Nuclear Energy 53, (2011): pp.1050–1055.
18. H. E. McCoy, “Type 304 Stainless Steel vs Flowing CO_2 at Atmospheric Pressure and 1100-1800°F,” Corrosion 21 (1965): pp.84-94.
19. W. R. Martin and J. R. Weir, “Influence of Chromium Content on Carburization of Chromium-Nickel-Iron Alloys in Carbon Dioxide,” J. Nucl. Mater. 16 (1965): pp.19-24.
20. B. A. Pint and J. R. Keiser, “Initial Assessment of Ni-Base Alloy Performance in 0.1 MPa and Supercritical CO_2,” JOM 67, 11 (2015): pp.2615-2620.
21. B. Pieraggi, "Calculations of Parabolic Reaction Rate Constants," Oxid. Met., 27 (1987): p.177.
22. Zs. Tökei, K. Hennesen, H. Viefhaus, H. J. Grabke, "Diffusion of Chromium in Ferritic and Austenitic 9-20 Wt.% Cr Steels," Materials Science Technology 16, (2000): pp.1129-1138.
23. G. Cao, V. Firouzdor, K. Sridharan, M. Anderson and T. R. Allen, “Corrosion of austenitic alloys in high temperature supercritical carbon dioxide,” Corrosion Science 60 (2012): pp.246-255.
24. V. Dheeradhada, A. Thatte, M. Karadge and M Drobnjak, “Corrosion of Supercritical CO2 Turbomachinery Components,” in Proceedings of the EPRI International Conference on Corrosion in Power Plants, Oct. 2016, San Diego, CA.
25. F. Rouillard, F. Charton and G. Moine, “Corrosion Behavior of Different Metallic Materials in Supercritical Carbon Dioxide at 550°C and 250 bars,” Corrosion 67, 9 (2011): p.095001.
26. L. Tan, M. Anderson, D. Taylor, T. R. Allen, “Corrosion of austenitic and ferritic-martensitic steels exposed to supercritical carbon dioxide,” Corrosion Science 53 (2011): pp.3273-3280.
27. G. H. Meier, W. C. Coons and R. A. Perkins, “Corrosion of Iron-, Nickel- and Cobalt-Base Alloys in Atmospheres Containing Carbon and Oxygen,” Oxidation of Metals 17 (1982): pp.235-262.
28. D. J. Young, T. D. Nguyen, P. Felfer, J. Zhang and J. M. Cairney, “Penetration of protective chromia scales by carbon,” Scripta Materialia 77 (2014): pp. 29–32.
29. C. T. Fujii and R. A. Meussner, “Carburization of Fe-Cr Alloys During Oxidation in Dry Carbon

Dioxide," J. Electrochem. Soc. 114 (1967): pp.435-442.
30. T. Gheno, D. Monceau and D. J. Young, "Kinetics of breakaway oxidation of Fe-Cr and Fe-Cr-Ni alloys in dry and wet carbon dioxide," Corrosion Science 77 (2013): pp.246-256.
31. R. P. Oleksak, G. R. Holcomb, C. S. Carney, L. Teeter, Ö. N. Doğan, "Effect of Surface Finish on High-Temperature Oxidation of Steels in CO_2, Supercritical CO_2, and Air," Oxidation of Metals 92 (2019): pp.525–540.